Photosensitizers

International Edition: DOI: 10.1002/anie.201501550
German Edition: DOI: 10.1002/ange.201501550

Combining Electron-Accepting Phthalocyanines and Nanorod-like CuO Electrodes for p-Type Dye-Sensitized Solar Cells**

Oliver Langmar, Carolina R. Ganivet, Annkatrin Lennert, Rubén D. Costa, Gema de la Torre, Tomás Torres,* and Dirk M. Guldi**

Abstract: *A route is reported for the synthesis of two electron-accepting phthalocyanines featuring linkers with different lengths as sensitizers for p-type dye-sensitized solar cells (DSSCs). Importantly, our devices based on novel nanorod-like CuO photocathodes showed high efficiencies of up to 0.191 %: the highest value reported to date for CuO-based DSSCs.*

Current developments in p-type dye-sensitized solar cells (DSSCs) focus on the discovery of novel electrodes and electron acceptors.[1,2] For electrodes, the most prominent material has been nickel(II) oxide (NiO), despite drawbacks such as low transparency, thickness of the electrodes, and low conductivity.[2] Some of these limitations can be overcome by the preparation of binary NiXO semiconductors, in which X is cobalt.[3] A viable alternative is the long overlooked copper(II) oxide (CuO), whose films feature higher conductivity, better charge-carrier mobility, and comparable valence-band energy relative to NiO films.[4,5] The most recent report on CuO-based p-type DSSCs dates back to 2008.[6] It is likely that state-of-the-art efficiencies as low as 0.011 % resulted in moderate interest. Recent improvements in the field of CuO-based p-type DSSCs are due to the use of copper delafossite ($CuXO_2$) electrodes, in which X is aluminum, chromium, or gallium.[7] Higher conductivities as well as lower valence-band energies, which cause higher open-circuit voltages (V_{oc}), are the major benefits of the latter electrodes. Other CuO nanostructures, such as nanorods and nanoplates, have not been explored to date. We demonstrate herein that DSSCs based on nanorod-like CuO electrodes outperform those with nanoparticle-like CuO and perform in a manner similar to those with $CuXO_2$.

In terms of dyes for p-type DSSCs, a myriad of organic and inorganic sensitizers, including triphenylamines,[8] perylenediimides,[9] perylene–bithiophene–triphenylamine triads,[10] porphycenes,[11] and ruthenium complexes,[12] have been designed and probed. Notably, the use of porphyrinoids has led to the most efficient n-type DSSCs to date.[13,14] Key merits of porphyrins, and in particular of synthetically related phthalocyanines (Pcs),[15,16] are their exceptional light-harvesting features and their facile functionalization with either electron donors or electron acceptors, thus underlining their potential for DSSCs.

Tuning of the physicochemical features of phthalocyanines through the placement of electron-withdrawing substituents at their periphery to create new electron-accepting dyes[17–19] complements our research on nanorod-like CuO electrodes. Notably, the synergy of nanorod-like CuO DSSCs and electron-accepting Pcs enabled the construction of p-DSSCs with efficiencies as high as 0.103 % and 0.191 % with iodine- and cobalt-based electrolytes, respectively. The latter value is the highest ever reported for a pure CuO-based DSSC. The design and synthesis of two novel zinc phthalocyanines, **ZnPc1** and **ZnPc2** (Scheme 1), for the sensitization of CuO nanorods were driven by several requirements. First, six electron-withdrawing alkyl sulfonyl groups were attached at the phthalocyanine periphery to render them electron accepting. Second, branched rather than linear alkyl chains were used to suppress aggregation on the surface of CuO nanorods. Third, either directly linked (in **ZnPc1**) or conjugated carboxylic acid anchoring groups (in **ZnPc2**) were attached to facilitate charge injection.

ZnPc1 and **ZnPc2** were synthesized in several steps in moderate yield (Scheme 1; see the Supporting Information for more details). First, statistical condensation of 4,5-bis(2-ethylhexylsulfonyl)phthalonitrile **1** and either phthalonitrile **2** or **3** afforded zinc(II) phthalocyanines **4** and **5**, respectively.[20] For **ZnPc1**, two consecutive oxidation steps were necessary to transform the hydroxymethyl-substituted Pc **4** into the corresponding carboxylic acid, namely, reaction with periodinane in dimethyl sulfoxide (DMSO) to afford formyl derivative **6**, and treatment with $NaClO_2$ in water in the presence of sulfamic acid. In the case of **ZnPc2**, an initial Sonogashira coupling between the monoiodo derivative **5** and propargylic alcohol afforded the hydroxypropargyl-substituted Pc **7**. The latter was oxidized by the same two-step procedure used for the conversion of **4** into **ZnPc1**. All final products and the corresponding intermediates were fully characterized by spectroscopic and electrochemical means.

[*] O. Langmar, A. Lennert, Dr. R. D. Costa, Prof. D. M. Guldi
Department of Physical Chemistry and Pharmacy, Interdisciplinary Center for Molecular Materials, University of Erlangen-Nürnberg
Egerlandstrasse 3, 91058 Erlangen (Germany)
E-mail: ruben.costa@fau.de
dirk.guldi@fau.de
C. R. Ganivet, Dr. G. de la Torre, Prof. T. Torres
Departamento de Química Orgánica
Universidad Autónoma de Madrid
C/Francisco Tomás y Valiente 7, 28049 Madrid (Spain)
E-mail: tomas.torres@uam.es

[**] We thank the German Science Council (DFG) for financial support in the framework of the Cluster of Excellence "Engineering of Advanced Materials (EAM)", the MINECO, Spain (CTQ2014-52869-P), the Comunidad de Madrid, Spain (FOTOCARBON, S2013/MIT-2841), and the European Union within FP7-ENERGY-2012-1 (Nr. 309194-2, GLOBASOL).

Supporting information for this article is available on the WWW under http://dx.doi.org/10.1002/anie.201501550.

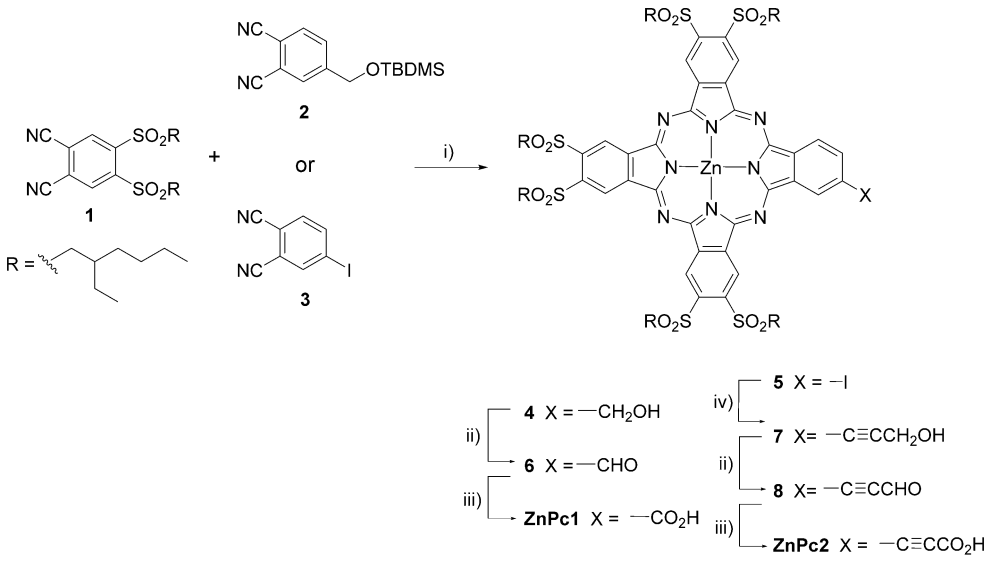

Scheme 1. Synthesis of **ZnPc1** and **ZnPc2**. Reaction conditions: i) $Zn(OAc)_2$, *o*-DCB/DMF (3:1), 170 °C, Ar, 18 h; ii) IBX, DMSO/THF; iii) H_3NSO_3/H_2O followed by $NaClO_2$; iv) propargyl alcohol, $[Pd(PPh_3)_2Cl_2]$, CuI, NEt_3, THF. *o*-DCB = *o*-dichlorbenzene, DMF = *N*,*N*-dimethylformamide, IBX = 2-iodoxybenzoic acid, TBDMS = *tert*-butyldimethylsilyl.

The absorption and fluorescence spectra of **ZnPc1** and **ZnPc2** were red-shifted by 25 nm as compared to those observed for a tetra-*tert*-butyl-substituted ZnPc reference, **ttb-ZnPc**, and exhibited slightly lower extinction coefficients (Figure 1). Furthermore, **ZnPc1** and **ZnPc2** showed split Q-bands (see Table S1 in the Supporting Information) as a result of their asymmetric functionalization.

Next, we performed cyclic voltammetry experiments to probe the electron-accepting character of **ZnPc1** and **ZnPc2** (see Figure S1 in the Supporting Information). Four quasi-reversible reductions at −0.94, −1.45, −1.82, and −2.06 V for **ZnPc1** and at −0.94, −1.36, −1.82, and −2.03 V for **ZnPc2** were complemented by one quasireversible oxidation at +0.72 V for **ZnPc1** and +0.77 V for **ZnPc2** (all values are given versus Fc/Fc^+). As compared to **ttb-ZnPc**, with a lowest reduction at −1.4 V and lowest oxidation at +0.1 V,[17] **ZnPc1** and **ZnPc2** should be better electron acceptors but poorer electron donors. We determined LUMO energies for **ZnPc1** and **ZnPc2** of −0.30 V versus NHE.[21] Considering that the redox potentials of the I^-/I^-_3 and Co^{2+}/Co^{3+} couples are 0.34 and 0.22 V, respectively, versus NHE,[22] **ZnPc1** and **ZnPc2** should be effectively regenerated in p-type DSSCs (see Figure S2). Moreover, the low-lying HOMOs of these compounds, that is, +1.36 V for **ZnPc1** and +1.41 V for **ZnPc2** versus NHE, imply efficient electron flow from the valence band (VB) of CuO into the corresponding HOMOs (see below).

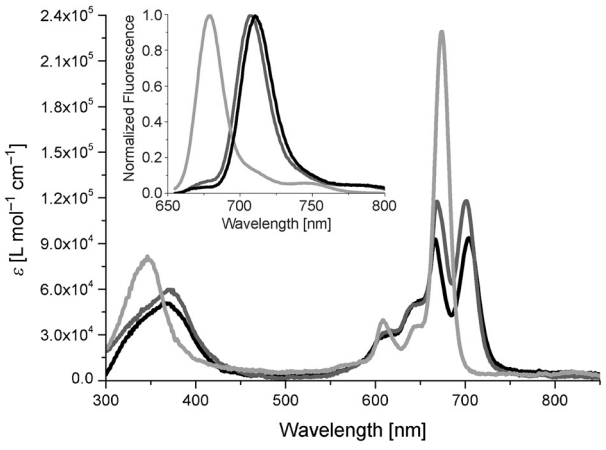

Figure 1. Absorption and fluorescence (inset) spectra of **ZnPc1** (black), **ZnPc2** (dark gray), and **ttb-ZnPc** (light gray) in EtOH (2.3×10^{-7} M).

Next, we assembled cells consisting of nanorod-like CuO as p-type electrodes and **ZnPc1/ZnPc2** as photosensitizers. In particular, we prepared the electrodes by doctor blading a paste of nanorod-like CuO diluted with ethylcellulose in ethanol, followed by sintering at 300 °C (see the Supporting Information for more details).[23] The crack-free mesoporous morphology and rodlike shape of CuO after calcination were corroborated by scanning electron microscopy (see Figure S3). The Fermi level energy of 0.55 V was determined in Kelvin probe microscopic experiments. As an approximation, we used this value (in agreement with a previously described approach) as the VB energy.[24] Furthermore, diffuse reflectance assays were used to determine a band-gap energy (E_g) of around 1.61 eV (see Figure S4).[25] With this information in hand, we calculated the energy position of the conduction band (CB) from the equation $E_{CB} = E_{VB} - E_g$ as −1.06 V versus NHE (see Figure S2). First, the HOMOs are placed 0.81 V (**ZnPc1**) and 0.86 V (**ZnPc2**) below the VB of the electrode. Such driving forces ensure an efficient electron flow from the electrodes to the photoexcited ZnPcs. Second, upon excitation, recombinations between the LUMO and the CB are unlikely. Finally, the electrolyte levels are 0.5–0.6 V below those of the corresponding LUMOs (see above), thus ensuring efficient dye regeneration. The p-type DSSCs were completed with Pt as the counter electrode and either LiI/I_2 (1:0.4) in a 50:50 (v/v) mixture of acetonitrile and 3-methoxypropionitrile or Co^{2+}/Co^{3+} (0.01:0.1) in the form of cobalt di-*tert*-butyl bipyridine hexafluorophosphate ($[Co(dtb\text{-}bpy)_3][PF_6]_{2/3}$) in acetonitrile as the electrolyte (see the Supporting Information for details).

The photocurrent density versus applied voltage (*J*–*V*) and the incident-photon-to-current efficiency (IPCE) spectra are shown in Figures 2 and 4, respectively, and the figures of merit are gathered in Table 1. The time dependences of the adsorption kinetics are important. For example, the efficiency

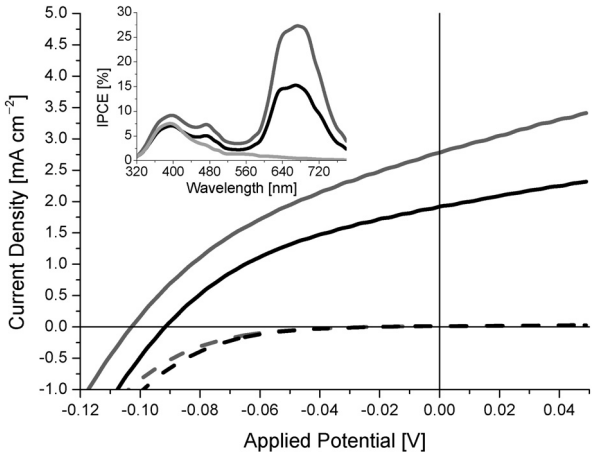

Figure 2. Current density versus applied potential under 1 sun and AM 1.5 conditions (solid line) and in the dark (dashed line) for **ZnPc1** (black) and **ZnPc2** (dark gray) devices with an iodine-based electrolyte. Inset: IPCE spectra of both kinds of devices as compared to that of a nonsensitized cell (light gray).

Table 1: Device performance under 1 sun and AM 1.5 conditions for **ZnPc1** and **ZnPc2**.

Dye	Electrolyte	V_{oc} [mV]	J_{sc} [mA cm^{-2}]	FF	η [%]	IPCE [%] at 670 nm
ZnPc1	I^-/I_3^-	93	1.93	0.38	0.067	15.4
ZnPc2	I^-/I_3^-	102	2.78	0.36	0.103	27.4
ZnPc1	Co^{2+}/Co^{3+}	224	1.99	0.32	0.141	14.9
ZnPc2	Co^{2+}/Co^{3+}	251	2.35	0.32	0.191	20.5

(η) started to rise before plateauing at around 60 min of ZnPc uptake (see Figure S5). The same trends were observed for the short-circuit current densities (J_{sc}) and the open-circuit voltages (V_{oc}). Similar concentrations of 1.38×10^{-8} and 1.39×10^{-8} mol cm^{-2} were derived for **ZnPc1** and **ZnPc2**, respectively, in desorption experiments, thus ensuring the comparability of the figures of merit.

As a starting point, we probed I^-/I^-_3 devices under 1 sun illumination and AM 1.5 conditions. **ZnPc2** devices showed higher V_{oc} and J_{sc} values than **ZnPc1** devices (102 versus 93 mV and 2.78 versus 1.93 mA cm^{-2}). In contrast, the fill factors (FF) were nearly the same, thus leading to overall efficiencies of 0.103 and 0.067 % for **ZnPc2** and **ZnPc1**, respectively. In line with these results, the IPCE value at 670 nm for **ZnPc2** (27.4 %) was around 78 % higher than that found for **ZnPc1** (15.4 %). Interestingly, the overall efficiency trend corresponds to that observed in n-type DSSCs sensitized by electron-donating ZnPcs featuring the same carboxylic linkers.[16]

Comparable conditions, in terms of dye loading, electrode thickness, and electrolyte composition, as well as differences in the J_{sc} and IPCE values, point to a linker-dependent injection and/or recombination processes. In **ZnPc2** the carboxylic linker is connected through a carbon–carbon triple bond, whereas the linker is directly connected in **ZnPc1** (Scheme 1). In general, the nature of the linker determines both the dye–electrode distance and the orientation of the dye relative to the surface.[26] Both factors seem to govern the injection and recombination kinetics, whereas thermodynamic differences between **ZnPc1** and **ZnPc2** can be ruled out (see above).

Considering the opaqueness of the CuO electrode, we turned to electrochemical impedance spectroscopy (EIS). The application of different voltages to change between short-circuit current density and open-circuit voltage conditions is useful in probing the aforementioned processes in p-type DSSCs.[27,28] In Nyquist plots under V_{oc} and J_{sc} conditions (see Figure S6), two semicircles, which relate to the resistance across the platinum/electrolyte interface in the high-frequency region and the dye/electrode/electrolyte interface in the low-frequency region, were discernable.[27] From the corresponding electrical-circuit model (see Figure S7), we derived the resistances and capacitances (Figure 3; see also Table S2).

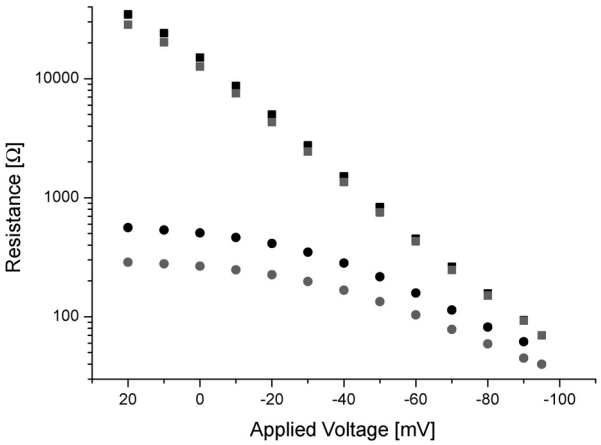

Figure 3. Resistance versus applied voltage for **ZnPc1** (black) and **ZnPc2** (gray) devices in the dark (squares) and under illumination (circles).

EIS measurements under dark conditions give insight into recombination processes between the electrode and the electrolyte.[27] Figure 3 shows that the recombination resistance (R_{rec}) increases with decreasing voltage. Within the voltage range, slightly lower resistances towards recombination with the I^-/I_3^- redox couple are noted for **ZnPc2** devices. In **ZnPc2** devices, larger dye-to-electrode distances facilitate interactions with the redox couple, as the electrode surface is more exposed to the polyiodide species. The IPCE spectra in Figure 2 substantiate this trend: **ZnPc2** devices feature in the high-energy region, which is dominated by the excitation of CuO and/or the redox couple. The observed IPCE values are slightly higher ($\leq$2 %) than those found for **ZnPc1** devices.

EIS measurements under illumination showed that several different contributions impact the charge-transfer resistance (R_{CT}). Besides electrode-to-electrolyte recombination processes, charge injection from the electrode to the dye and charge transport throughout the electrode play major roles.[29] Again, a linear increase in R_{CT} with decreasing voltage was noted before a plateau was reached at around J_{sc} conditions (Figure 3). A similar trend was recently reported for NiO-based DSSCs.[28]

Overall, **ZnPc2** devices give rise to lower R_{CT} values throughout the entire voltage range as compared to **ZnPc1** devices, thus indicating better charge injection and charge transport in the former. At V_{oc} conditions, recombination across the electrode/electrolyte interface dominates owing to the lack of external currents. In line with EIS observations in the dark, the resistance towards recombination with I^-/I^-_3 is lower for **ZnPc2** (40.0 Ω) than for **ZnPc1** (61.8 Ω). At the J_{sc} value and under forward conditions, the absence of recombinations enables the relationship between R_{CT} and the charge injection, that is, from the electrode to the dye, to be established. The R_{CT} value of **ZnPc1** (506.3 Ω) is nearly twice that of **ZnPc2** (266.4 Ω), which points to better charge injection for the latter. The IPCE spectra are helpful in this regard, since photocurrents at around 670 nm (due to dye excitation) are nearly twice as high for **ZnPc2**. Because of the lack of photoactivity of the electrolyte in the low-energy region, only contributions from the charge injection can be used to rationalize the superior performance of devices featuring **ZnPc2**.

Additional device properties, namely the chemical capacitance (C_μ), the charge-collection efficiency (η_{cc}), the effective diffusion length (L_{eff}), and the effective diffusion coefficient (D_{eff}), were determined for all devices (see Figure S8).[28,30] Briefly, C_μ directly correlates with the density of injected holes at the electrode. A higher rate of charge injection increases the hole density, thus affording higher V_{oc} and C_μ values.[31] In agreement with this notion, higher V_{oc} values, higher C_μ values, and superior charge injections were observed for **ZnPc2**. The improved η_{cc} values in devices with **ZnPc2** can also be explained in terms of the rate of charge injection across the electrode/dye interface, which was twice as efficient in **ZnPc2**, as reflected in longer L_{eff} values and higher D_{eff} values than those observed for **ZnPc1** devices.

The major limitation of our devices is related to the low V_{oc} values, since the J_{sc} values are comparable to those of $CuXO_2$-based DSSCs.[7] The use of $[Co(dtb\text{-}bpy)_3][PF_6]_{2/3}$ as the electrolyte is the most efficient way to overcome this limitation.[22] Under 1 sun illumination and AM 1.5 conditions, **ZnPc2** DSSCs revealed higher V_{oc} and J_{sc} values (251 mV and 2.35 mA cm^{-2}) than those of **ZnPc1** DSSCs (224 mV and 1.99 mA cm^{-2}; Figure 4 and Table 1). Importantly, IPCEs for **ZnPc2** at 670 nm were nearly 5.5% higher than those for **ZnPc1**. More relevant is the increase in the V_{oc} values by almost 150% when comparing cobalt-based devices with iodine-based devices, thus leading to η values of 0.191 and 0.141% for **ZnPc2** and **ZnPc1**, respectively. EIS assays under V_{oc} and J_{sc} conditions are also in line with the trends noted for devices with iodine-based electrolytes (see Figure S9 and Table S3). **ZnPc2** devices revealed in comparison to **ZnPc1** devices a slightly higher recombination with the electrolyte, as well as a better charge injection.

In conclusion, two novel electron-accepting ZnPcs, **ZnPc1** and **ZnPc2**, which differ in their linker length, were synthesized and characterized by means of steady-state photophysical as well as electrochemical techniques. Both ZnPcs present significant absorption cross-sections throughout the visible part of the solar spectrum and excellent electron-accepting behavior. These features prompted us to use them as photosensitizers in p-DSSCs based on nanorod-like CuO electrodes, which have never been explored. To this end, devices featuring **ZnPc1** and **ZnPc2** were tested under either 1 sun and AM 1.5 conditions or dark conditions and yielded maximum efficiencies of up to 0.103% and 0.191% for iodine- and cobalt-based electrolytes, respectively. These values are the highest reported efficiencies for pure CuO p-type DSSCs. Furthermore, EIS assays corroborate that **ZnPc2**, featuring a carboxyethynyl anchor, is a more suitable photosensitizer than **ZnPc1**, in which the carboxylic acid anchor is directly linked to the macrocycle. The presence of the ethynyl bridge enhances the electronic coupling between ZnPc and CuO, thus providing an optimum balance between charge injection and charge recombination. Future research will be focused on the further optimization and EIS characterization of p-type CuO devices, as well as the improvement of electron-accepting ZnPcs for p-type DSSC applications.

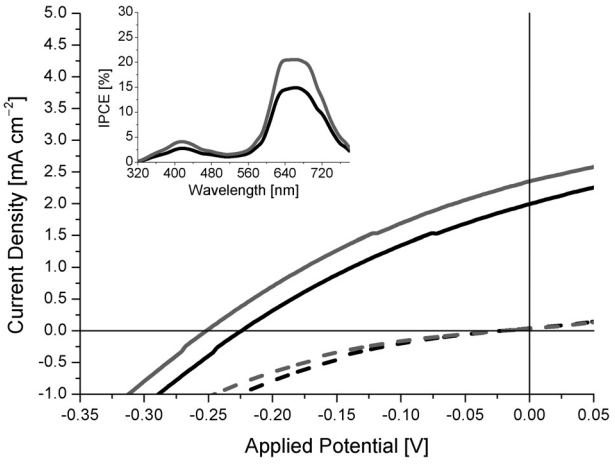

Figure 4. Current density versus applied potential under 1 sun and AM 1.5 conditions (solid line) and in the dark (dashed line) for **ZnPc1** (black) and **ZnPc2** (gray) devices with a cobalt-based electrolyte. Inset: IPCE spectra for both kinds of devices. The IPCE spectrum of the nonsensitized device is not shown, since a maximum of only 0.13% was measured at 400 nm.

Keywords: CuO electrodes · CuO nanorods · dye-sensitized solar cells · electrochemical impedance spectroscopy · zinc phthalocyanines

How to cite: *Angew. Chem. Int. Ed.* **2015**, *54*, 7688–7692
Angew. Chem. **2015**, *127*, 7798–7802

[1] F. Odobel, L. Le Pleux, Y. Pellegrinn, E. Blart, *Acc. Chem. Res.* **2010**, *43*, 1063–1071.
[2] F. Odobel, Y. Pellegrin, *J. Phys. Chem. Lett.* **2013**, *4*, 2551–2564.
[3] G. Natu, P. Hasin, Z. Huang, Z. Ji, M. He, Y. Wu, *ACS Appl. Mater. Interfaces* **2012**, *4*, 5922–5929.
[4] D. M. Jundale, P. B. Joshi, S. Sen, V. B. Patil, *J. Mater. Sci. Mater. Electron.* **2012**, *23*, 1492–1499.
[5] S. Makhlouf, M. Kassem, M. Abdel-Rahim, *J. Mater. Sci.* **2009**, *44*, 3438–3444.
[6] S. Sumikura, S. Mori, S. Shimizu, H. Usami, E. Suzuki, *J. Photochem. Photobiol. A* **2008**, *194*, 143–147.
[7] M. Yu, T. I. Draskovic, Y. Wu, *Phys. Chem. Chem. Phys.* **2014**, *16*, 5026–5033.

[8] P. Qin, H. Zhu, T. Edvinsson, G. Boschloo, A. Hagfeldt, L. Sun, *J. Am. Chem. Soc.* **2008**, *130*, 8570 – 8571.
[9] L. Le Pleux, A. L. Smeigh, E. Gibson, Y. Pellegrin, E. Blart, G. Boschloo, A. Hagfeldt, L. Hammarström, F. Odobel, *Energy Environ. Sci.* **2011**, *4*, 2075 – 2084.
[10] M. Weidelener, A. Mishra, A. Nattestad, S. Powar, A. J. Mozer, E. Mena-Osteritz, Y.-B. Cheng, U. Bach, P. Bäuerle, *J. Mater. Chem.* **2012**, *22*, 7366 – 7379.
[11] S. Feihl, R. D. Costa, W. Brenner, J. T. Margraf, R. Casillas, O. Langmar, A. Browa, T. E. Shubina, T. Clark, N. Jux, D. M. Guldi, *Chem. Commun.* **2014**, *50*, 11339 – 11342.
[12] Z. Ji, G. Natu, Y. Wu, *ACS Appl. Mater. Interfaces* **2013**, *5*, 8641 – 8648.
[13] M. Urbani, M. Grätzel, M. K. Nazeeruddin, T. Torres, *Chem. Rev.* **2014**, *114*, 12330 – 12396.
[14] S. Mathew, A. Yella, P. Gao, R. Humphry-Baker, B. F. E. Curchod, N. Ashari-Astani, I. Tavernelli, U. Rothlisberger, M. K. Nazeeruddin, M. Grätzel, *Nat. Chem.* **2014**, *6*, 242 – 247.
[15] J.-J. Cid, J.-H. Yum, S.-R. Jang, M. K. Nazeeruddin, E. Martínez-Ferrero, E. Palomares, J. Ko, M. Grätzel, T. Torres, *Angew. Chem. Int. Ed.* **2007**, *46*, 8358 – 8362; *Angew. Chem.* **2007**, *119*, 8510 – 8514.
[16] M.-E. Ragoussi, J.-H. Yum, A. K. Chandiran, M. Ince, G. de la Torre, M. Grätzel, M. K. Nazeeruddin, T. Torres, *ChemPhysChem* **2014**, *15*, 1033 – 1036.
[17] M.-E. Ragoussi, G. Katsukis, A. Roth, J. Malig, G. de la Torre, D. M. Guldi, T. Torres, *J. Am. Chem. Soc.* **2014**, *136*, 4593 – 4598.
[18] A. Roth, M.-E. Ragoussi, L. Wibmer, G. Katsukis, G. de la Torre, T. Torres, D. M. Guldi, *Chem. Sci.* **2014**, *5*, 3432 – 3438.
[19] B. Tylleman, G. Gbabode, C. Amato, C. Buess-Herman, V. Lemaur, J. Cornil, R. Gómez Aspe, Y. H. Geerts, S. Sergeyev, *Chem. Mater.* **2009**, *21*, 2789 – 2797.
[20] For the synthesis of **4**, a deprotection step is necessary after the cyclotetramerization reaction (see the Supporting Information).
[21] C. M. Cardona, W. Li, A. E. Kaifer, D. Stockdale, G. C. Bazan, *Adv. Mater.* **2011**, *23*, 2367 – 2371.
[22] E. A. Gibson, A. L. Smeigh, L. Le Pleux, L. Hammarström, F. Odobel, G. Boschloo, A. Hagfeldt, *J. Phys. Chem. C* **2011**, *115*, 9772 – 9779.
[23] S. Ito, T. N. Murakami, P. Comte, P. Liska, C. Grätzel, M. K. Nazeeruddin, M. Grätzel, *Thin Solid Films* **2008**, *516*, 4613 – 4619.
[24] C.-Y. Chiang, K. Aroh, N. Franson, V. R. Satsangi, S. Dass, S. Ehrman, *Int. J. Hydrogen Energy* **2011**, *36*, 15519 – 15526.
[25] V. Kumar, S. K. Sharma, T. Sharma, V. Singh, *Opt. Mater.* **1999**, *12*, 115 – 119.
[26] A. S. Hart, C. B. KC, H. B. Gobeze, L. R. Sequeira, F. D'Souza, *ACS Appl. Mater. Interfaces* **2013**, *5*, 5314 – 5323.
[27] Z. Huang, G. Natu, Z. Ji, P. Hasin, Y. Wu, *J. Phys. Chem. C* **2011**, *115*, 25109 – 25114.
[28] Z. Huang, G. Natu, Z. Ji, M. He, M. Yu, Y. Wu, *J. Phys. Chem. C* **2012**, *116*, 26239 – 26246.
[29] H. Choi, S. O. Kang, J. Ko, G. Gao, H. S. Kang, M.-S. Kang, M. K. Nazeeruddin, M. Grätzel, *Angew. Chem. Int. Ed.* **2009**, *48*, 5938 – 5941; *Angew. Chem.* **2009**, *121*, 6052 – 6055.
[30] M. Adachi, M. Sakamoto, J. Jiu, *J. Phys. Chem. B* **2006**, *110*, 13872 – 13880.
[31] J. Bisquert, *Phys. Chem. Chem. Phys.* **2003**, *5*, 5360 – 5364.

Received: February 17, 2015

